Materials Today: Proceedings xxx (xxxx) xxx

Contents lists available at ScienceDirect

Materials Today: Proceedings

journal homepage: www.elsevier.com/locate/matpr

Analysis of FSW welding parameters on mechanical welding properties in aluminum alloy AA 5083 plates using different tool geometries

C.R. Mahesha [a], N. Nithyanandan [b], K.V. Pradeep Kumar [c], Ravi Kanojia [d], Vipin Sharma [e], R. Satheesh Raja [f], G. Sasikala [g,*]

[a] Department of Industrial Engineering and Management, Dr. Ambedkar Institute of Technology, Bangalore, Karnataka 560056, India
[b] Department of Mechanical Engineering, Panimalar Engineering College, Chennai, Tamil Nadu 600123, India
[c] Department of Mechanical Engineering, M S Ramaiah Institute of Technology, Bengaluru, Karnataka 560054, India
[d] Department of Mechanical Engineering, Graphic Era Deemed to be University, Dehradun, Uttarakhand 248002, India
[e] Department of Mechanical Engineering, Sagar Institute of Research and Technology, Bhopal, Madhya Pradesh 462041, India
[f] Department of Marine Engineering, PSN college of Engineering and Technology, Tirunelveli, Tamil Nadu 627152, India
[g] Department of Mathematics, SRM Valliammai Engineering College, Kattankulathur, Chennai, Tamil Nadu 603202, India

ARTICLE INFO

Keywords:
Friction Welding
Heat source
Magnesium/ Aluminium
Modeling

ABSTRACT

Friction welding is based on a rotating tool that penetrates the line of union of the previously fixed and pressed pieces and moves along this line. It is a process of joining materials at low temperatures, in the solid state of metals, below their melting point. The heat generated by the friction of the tool at high rotation further dilutes the base material and flows towards the center of the tool, causing mechanical mixing, the shoulder of which causes the final stage of this material, already cooled. This article proposes to study the influence of the different parameters of FSW welding on the thermal characteristics of weld joints in aluminum and magnesium alloys, numerically. The simulation results confirmed that the temperature distribution is high from shoulder towards the borders of the parts and it was symmetrical with respect to the middle plane. The calculated maximum temperatures for magnesium and aluminum were 843.7 K & 702 K, respectively.

1. Introduction

Welding is one of the most popular and widely used means of assembling metal structures and without which several industrial applications would not have been possible [1,2]. This is why welding processes have been in constant development since the 19th century, going from torch welding to arc welding to laser welding. One of the developed and relatively recent processes is friction stir welding commonly known by FSW "Friction Stir Welding", which has many advantages particularly in the aeronautics and space sectors [3–5]. These industrial sectors require minimal weight in the structures, adequate mechanical properties, ease of implementation and reliable assemblies [6,7].

The FSW process was patented in the early 90 s by TWI (The Welding Institute) in Great Britain and consists of assembling materials in the solid phase (in the pasty range) using a specific cylindrical tool set in rotation [8,9]. The latter consists of a shoulder which is used to generate heat by friction and a pin which has the role of mixing the plasticized material to form the weld bead [10,11]. The pin enters the part until the shoulder is in contact with the face of the part to be welded then the tool begins its advance along a line of weld while keeping the temperature of the material lower than its Fusion point. This technology has many advantages over conventional processes. Indeed, the absence of fusion means the absence of solidification and recrystallization problems, there is less distortion of the material and therefore less residual stresses [12,13]. This process also allows the assembly of alloys that are difficult to weld by conventional techniques and represents an alternative to welding [14,15].

Several research projects have been carried out by the scientific community to better understand the characteristics and parameters influencing FSW welding [16–18]. However, the appropriate numerical analysis is mkissing in the accessible literature. This research has the novelty, which is mainly focused on the study of different influence parameters of FSW on the thermal characteristics of weld joints in aluminum and magnesium alloys, numerically.

* Corresponding author.
E-mail address: sasigmath83@gmail.com (G. Sasikala).

https://doi.org/10.1016/j.matpr.2023.08.095
Received 16 May 2023; Received in revised form 8 August 2023; Accepted 9 August 2023

2. Mathematical development

To solve the thermal problem of FSW welding, it is mainly necessary to know the amplitude of the flux absorbed by the parts to be welded. Thermal modeling based on the two thermal sources of FSW welding (friction and plastic deformations at the tool/part interfaces) has been the subject of several studies [19–21]. It presents an essential step for understanding the transfer of heat, the flow of material around the tool and the microstructural modification of the weld.

All of the thermal modeling work in FSW is based on the resolution of the heat conduction equation completed by the boundary conditions, appropriate initials and the model of the thermal source [14].

In our case, we chose the thermal model of [22] for the resolution of the friction stir welding problem.

2.1. General assumptions

The considered thermal problem is managed by the general heat transfer equation in 3D. We therefore consider the following simplifying assumptions [23,24]:

- The system of coordinates considered is three-dimensional (o, x, y, z) and assumed to be mobile and linked to the axis of the tool, the physical description is therefore in Eulerian configuration and the regime becomes quasi-stationary of type (conduction / convection).
- The tool pin is assumed to be cylindrical.
- The conduction losses at the contact surfaces between the part to be welded with the lower support are assumed under a convective transfer mode having a specific heat transfer coefficient.
- Losses on other surfaces of the part are assumed only by natural convection where the exchange coefficient is h∞ (of ambient air).
- The heat due to the plastic deformation of the material to be welded by the effect of the FSW tool, is assumed to be negligible, comparing with the heat generated by friction.
- The local temperature cannot exceed the melting temperature T_f.
- Heat transfer by radiation is negligible.

2.2. Equation of heat transfer in the parts to be welded

Considering the previous assumptions [25], the heat transfer equation in the room at weld with the positive ox axis as welding direction, is:

$$\frac{\partial}{\partial t}(\rho cT) = \frac{\partial}{\partial x}\left(K_x\frac{\partial T}{\partial x}\right) + \frac{\partial}{\partial y}\left(K_y\frac{\partial T}{\partial y}\right) + \frac{\partial}{\partial z}\left(K_x\frac{\partial T}{\partial z}\right) + v\frac{\partial}{\partial x}(\rho cT) \quad (1)$$

Where: ρ is the density of the material, K(x, y, z) is the thermal conductivity in the different directions, 'c' is the heat capacity, *v* is the feed rate of the tool in the part and T temperature.

2.3. Heat source model

According to the bibliography, there are two major sources of heat: heat at the interface of the pin / part to be welded and the heat at the shoulder / part to be welded interface [26,27]. The heat generated locally between the shoulder and the surface of the part in a surface element with a distance Ri can be calculated as follows [28,29]:

$$q_S = 2\cdot\pi\cdot\mu\cdot Fn\cdot R_i\cdot\frac{\omega}{60\cdot A_S} \quad (2)$$

Where μ is the coefficient of friction which varies with T during the FSW process, for this model initially μ is assumed = 0.4, F_n is the normal force, Ri is the distance between the axis of rotation of the tool at one point 'i' at the interface below the shoulder, ω is the tool rotational speed (RPM), As is the friction surface of the shoulder.

The heat generated locally at the pin/part interface consists of 3 parts [29,30]: (a) heat generated by shearing of the material, (b) heat generated by friction on the thread surface of the pin, (c) heat generated by friction on the bottom surface of the pin.

In this work, we are neglecting the first and third parts (a and c) compared to part (b). Colegrove gave the following model of this heat source [2,31]:

$$Q_p = 2\pi r_p HK\overline{Y}\frac{V_m}{\sqrt{3}} + \frac{2\mu\overline{Y}\pi r_p HV_{rp}}{\sqrt{3(1+\mu^2)}} + \frac{4F_n\mu V_m\cos\theta}{\pi} \quad (3)$$

And so equation (3) becomes:

$$q_p = \frac{2.\mu.\overline{Y}\pi.r_p.H.V_{rp}}{\sqrt{3(1+\mu^2)}} \quad (4)$$

Where, $\overline{Y}$ is the average shear stress of the material, *rp* is the radius of the tool pin, H is the thickness of the part to be welded, μ is the coefficient of friction, F_n is the translational force during welding.

2.4. Initial and boundary conditions

To solve the heat transfer equation numerically or analytically it is necessary first correctly set the initial and boundary conditions [15]. Initial calculation condition: the temperature in the initial state of the tool and the parts to be welded is:

$$T(x, y, z, t) = T_0 = 300K \quad (5)$$

The boundary conditions at the shoulder / part to be welded and pin / part to be welded interfaces are respectively [15,32]:

$$k\left(\frac{\partial T}{\partial n}\right)_\Gamma = q_S \quad (6)$$

$$k\left(\frac{\partial T}{\partial n}\right)_\Gamma = q_W \quad (7)$$

Where q_S and q_W are the heat flows generated at the shoulder/workpiece and pin/workpiece interfaces. Heat transfer at the contact interface of the part to be welded with the lower support is given by [15]:

$$k\left(\frac{\partial T}{\partial n}\right)_\Gamma = \overline{h}(T - T_0) \quad (8)$$

The type of heat exchange between the part to be welded and its surrounding environment is convective, it is modeled by a thermal convection coefficient h_∞:

$$k\left(\frac{\partial T}{\partial n}\right)_\Gamma = h_\infty(T - T_0) \quad (9)$$

Due to the symmetry of the two parts to be welded on either side of the vertical plane of the weld (parallel to the weld bead, Fig. 1), it can be assumed that the temperature gradient in the direction transverse to the weld is zero along this plane. This condition is not applicable for heterogeneous welding.

$$\left(\frac{\partial T}{\partial y}\right)_{xsym} = 0 \quad (10)$$

3. Numerical simulation

The equations managing the phenomenon are solved by the finite element method (a method which discretizes the partial differential equations by obtaining a system of algebraic equations) then an iterative numerical method is used to solve the system and obtain the solution of the thermal problem [33,34]. For this we use COMSOL software.

In this part of modeling principle (Fig. 2), we present the steps to follow to model the phenomenon of heat transfer during FSW welding for the different welding cases: homogeneous (AL-Al/Mg-Mg) and heterogeneous (Al-Mg/Mg-Al).

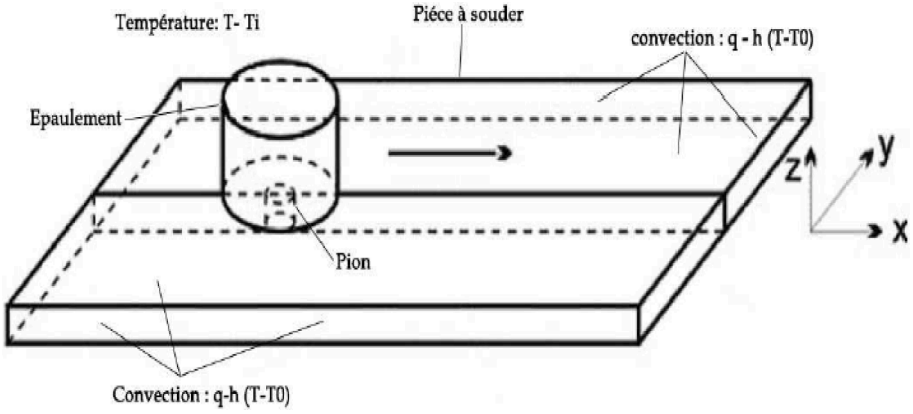

Fig. 1. Diagram showing the initial and boundary conditions of FSW welding.

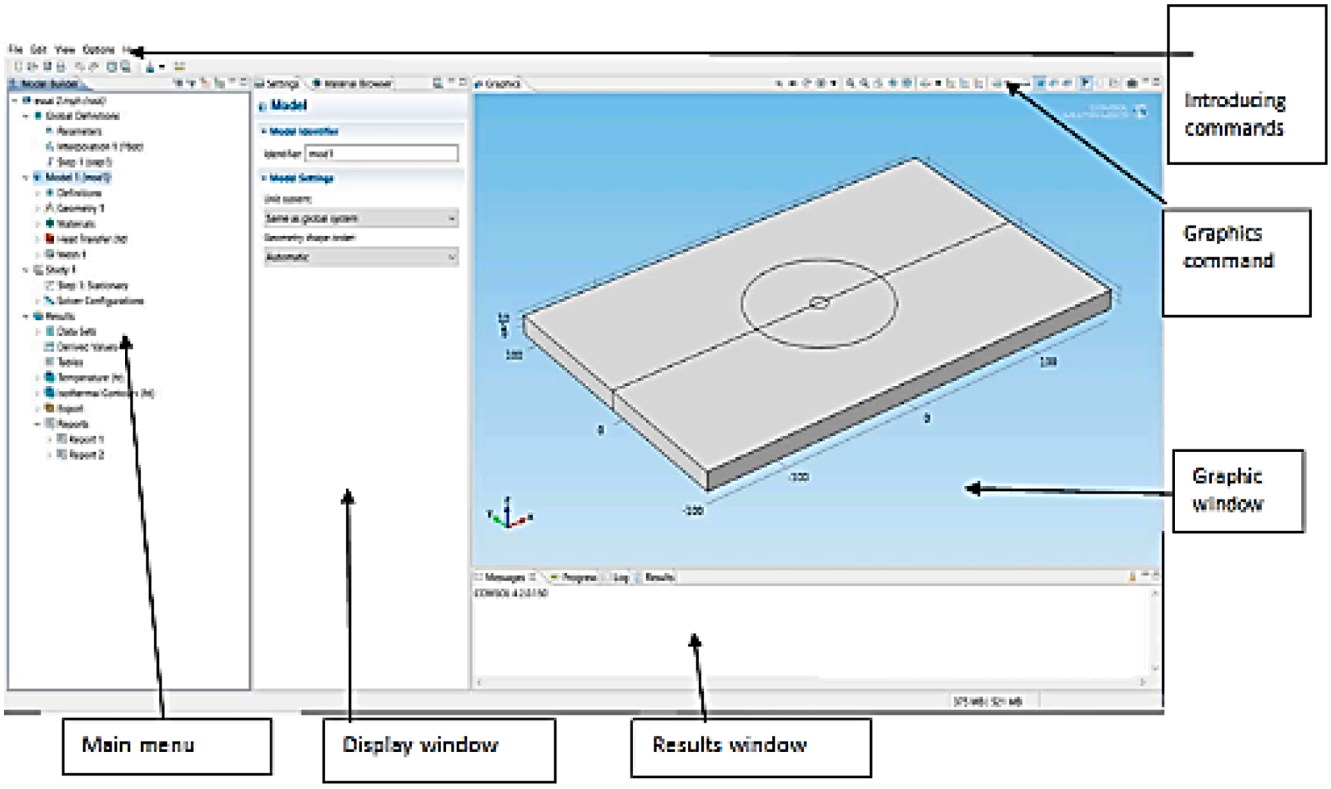

Fig. 2. COMSOL software interface (window and command menu).

3.1. Choose the type of study

- Choose the dimensions of the space in which we are going to work
- Choose the type of physical phenomenon studied
- Choose the type of study
- Introduce the parameters of the phenomenon into the program by clicking with the right on
- GlobalDefinitions > Parameters.
- Introduce the function that defines the variation of shear stress as a function of temperature by clicking with the right on Global Definitions > Function > Interpolation.
- Define the calculation time and step by right-clicking on Global Definitions > Function > Step

3.1.1. Define the geometry

The numerical simulation is carried out on sheets of aluminum alloy Al 2024-T4 and Magnesium AZ31B, 320 mm long, 102 mm wide and 12.7 mm thick each, assembled in pairs, in different cases [1,6].

The tool is made of H-13 steel. The pin geometry is cylindrical with a height of 12 mm and a radius of 6 mm. The shoulder of the tool is also cylindrical with a height of 30 mm above the plates to be welded and a radius of 25 mm [10].

- To draw the two plates to be welded you must: click with the right on Geometry 1 > Block then inject the dimensions of each plate and to display it select Build Selected.
- To draw the shoulder and the pin: the same as for the plates except that we choose Cylinder instead of Block then inject the correct dimensions.

To complete the geometry just right click on From Union and choose Build Selected (Fig. 3).

3.1.2. Define heat sources

- To define the surface heat source equations of the shoulder and the pin, click on with the right Definitions > Variables, then select the boundary corresponding to each equation [6].
- Define the initial and boundary conditions:
- To enter the initial temperature of the parts, expand the Heat Transfer in Solids > Initial Values 1 section.
- To define the speed of translation: click with the right on Heat Transfer in Solid 1 > Translational Motion (in our case it is the sheets which are moving with respect to the tool because we are in an Eulerian frame) [1,10].
- For the top and side surfaces as well as the faces of the shoulder in contact with
- the air we have a convection whose coefficient is h_upside (ambient air), we introduce it by clicking with the right on Heat Transfer in Solid 1 > Heat flux then select the corresponding faces without forgetting to define T0 in as external temperature [10].
- in the same way for the faces of the bottom it is enough to change the coefficient with h_downside (of the table of the machine).
- To define the boundary condition at the shoulder/workpiece interface: right-click on Heat Transfer in Solid > Boundry Heat Source after selecting the corresponding faces and introduce the variable describing the shoulder/workpiece heat source.
- Similarly to define the boundary condition at the pin/part to be welded interface.
- For the downstream transverse face of the plates, a limit condition is imposed on it by clicking with the right on Heat Transfer in Solid > Outflow.
- For the upstream transverse face of the plates, an initial temperature T0 is imposed on it by clicking with the right on Heat Transfer in Solid > Temperature 1.

3.1.3. Define materials

To define the material of each part you must: go to Material Browser, select the desired material and then assign it to the corresponding geometric domain [35,36].

- the tool is H13 steel (UNS T20813) [solid].

Regarding plate materials (Fig. 4, Fig. 5, and Fig. 6), we tested four configurations with Aluminum 2024-T4 and Magnesium AZ31B alloys: two homogeneous Al-Al / Mg-Mg and two heterogeneous Al-Mg / Mg-Al, to define them. repeat the same steps as for the tool.

3.1.4. Define the mesh

To create the mesh, we choose the Free Tetrahedral option in the mesh 1 menu, and we choose an Extremely Fine dimensioning in the size menu to have a more refined mesh around the tool in order to better capture the thermal gradient in this area [10]. The number of degrees of freedom (degree of freedom to solve) obtained is: 109749.

3.1.5. Solution

As our problem is quite light, the solver configuration defaults the software is enough to solve it [6,10].

To configure the solver: expand the menu Study 1 > Solver Configurations > Solver 1 > Stationary Solver 1 and right-click on Direct > Enable. To launch the calculation: click with the right on Study 1 and choose Compute.

3.1.6. Convergence

The resolution of the problem took about 77 s and gave a decreasing convergence curve. Convergence is reached after 8 iterations with an error of 10^{-5} (Fig. 7).

4. Results and discussion

According to the Fig. 8 and Fig. 9, the temperatures are distributed gradually from the shoulder towards the borders of the parts, we notice that the temperature distribution is symmetrical with respect to the middle plane (x,z) [1,6]. The calculated maximum temperatures are lower than the melting temperatures of the materials in both cases, for magnesium $T_{max} = 843.7$ K (about 91% of T_f) for aluminum $T_{max} = 702$ K (about 75% of T_f). These maximum temperatures are located in the mixed zone and shift towards the rear of the center of the tool due to the movement of translation and rotation of the tool.

Fig. 8 and Fig. 9 show the temperature distribution at depth in the plane (y,z) under the shoulder and around the pin. The maximum temperatures decrease from the shoulder towards the lower surface of the plates, thus creating a maximum zone in the form of an inverted quasi-cone with a slight asymmetry [10]. This is the result of the translation movement of the tool and the rotation of the material around the pin, which generates the two sides of advance AS (Advancing Side) and withdrawal (Retreating Side).

The chemical and MC and the PS of the residue are favorable

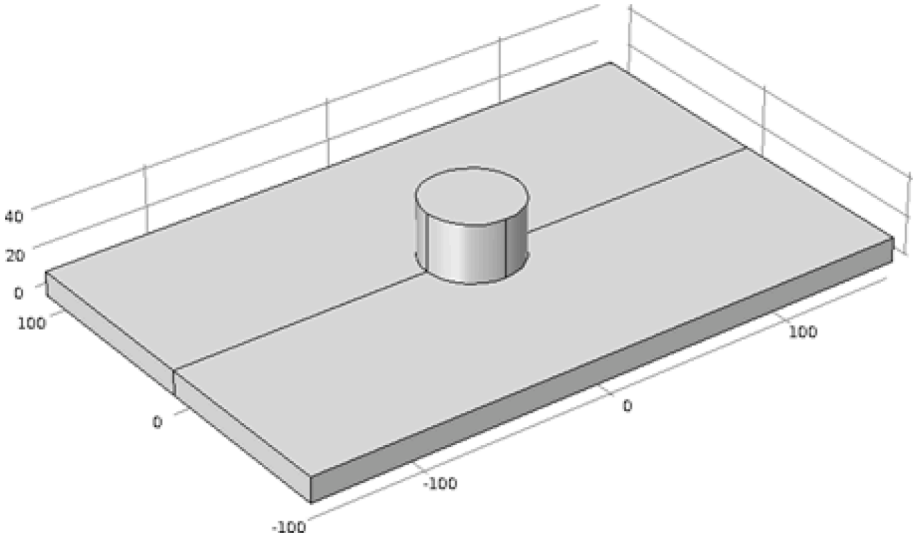

Fig. 3. The complete geometry.

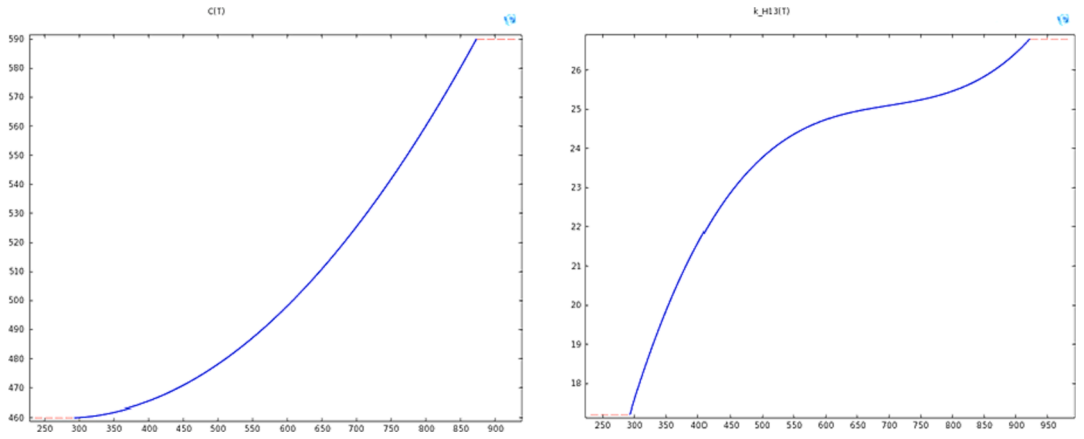

Fig. 4. Specific heat at constant pressure Cp and thermal conductivity k as a function of temperature in K for H13 steel.

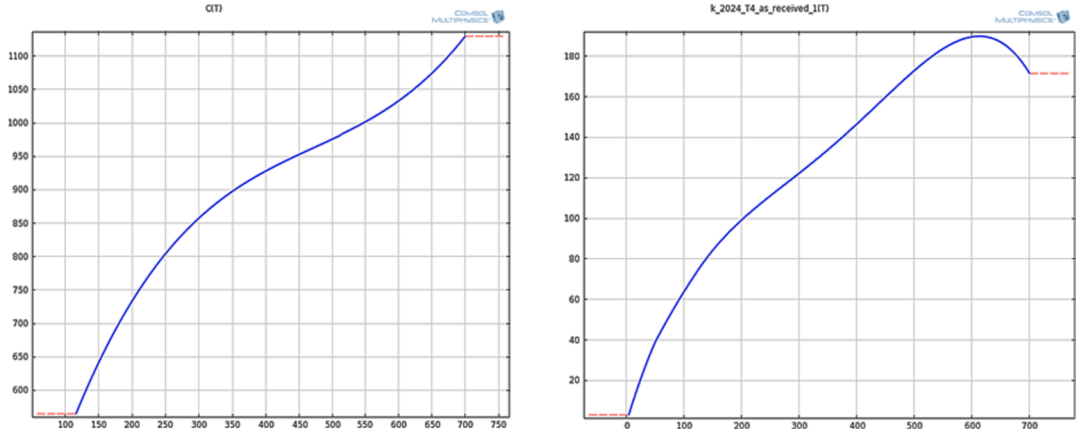

Fig. 5. Specific heat at constant pressure Cp and thermal conductivity k as a function of temperature in K for 2024-T6 Aluminum alloy.

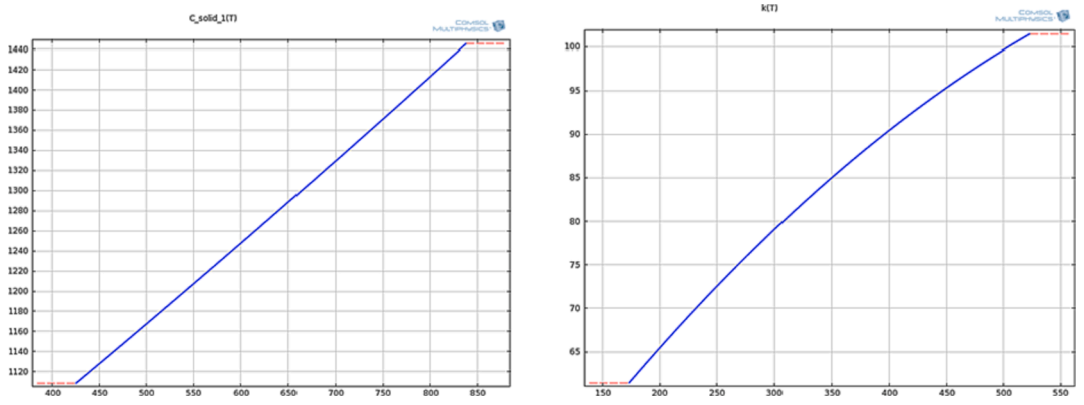

Fig. 6. Specific heat at constant pressure Cp and thermal conductivity k as a function of temperature in K for Magnesium AZ31B alloy.

characteristics for its use in CRs. The residue has significant amounts of alkaline oxides (7.8%) and alkaline earth oxides (9.0%), which can act as fluxes during the CR firing stage. The fluxes provide greater formation of the liquid phase, consequently, it helps to close the porosity between the particles, increasing the relative density of the sintered material [1]. The residue with smaller PS can improve the densification of the CR body by forming a greater amount of liquid phase during firing. It is concluded, therefore, that the residue from the processing of OS can be used in clayey CRs. The benefit of using waste as fluxes in CRs is providing an ecological and economic destination for waste from the processing of OS.

The heterogeneous welding of Aluminum alloys to Magnesium alloys using TIG, MIG, FE (electron beam) or even Laser welding processes has been the subject of several studies, on the other hand few have been interested in welding, using FSW to make this weld. In this work, we were interested in this idea by studying the heat transfer during FSW welding of Aluminum 2024-T4 to Magnesium AZ31B, which represents the first step for the study of weld quality.

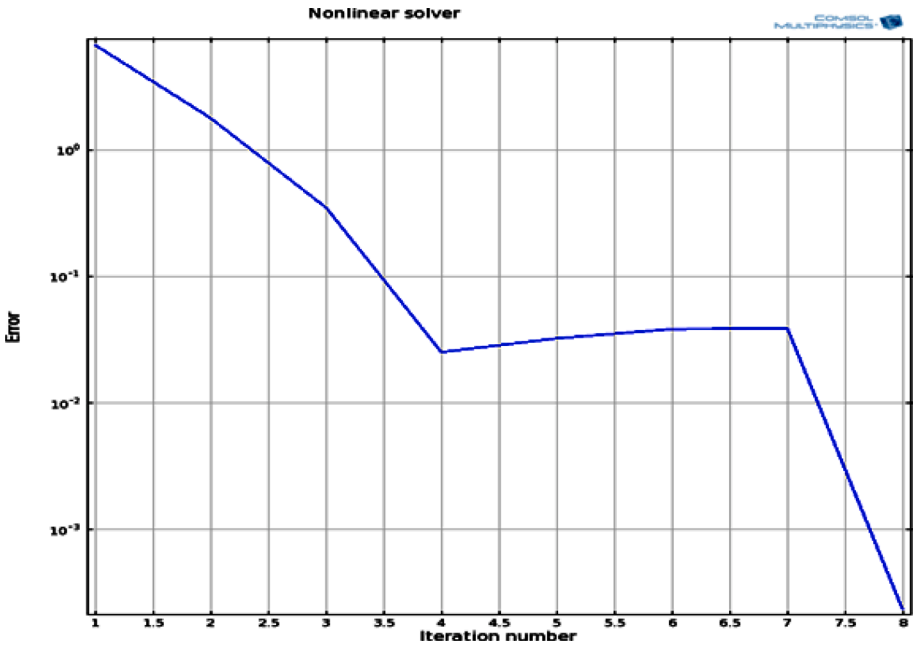

Fig. 7. Curve of evolution of the convergence according to the iterations.

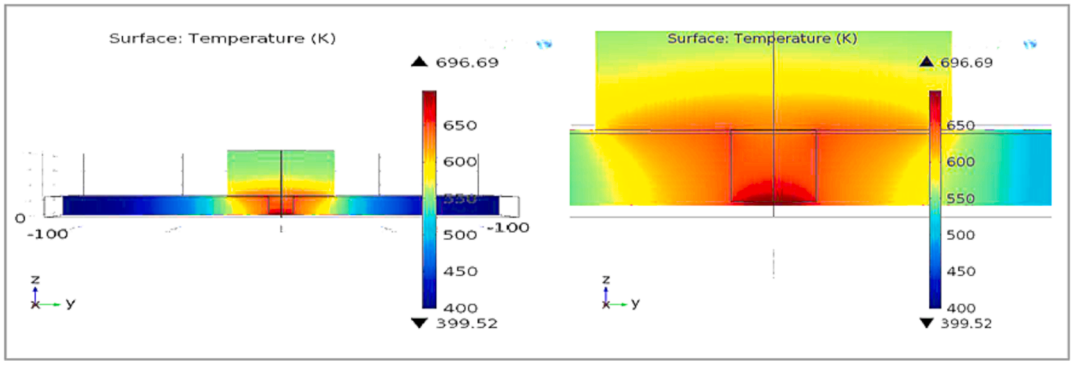

Fig. 8. Temperature distribution in the xz plane, and temperature distribution during welding for Al-Al.

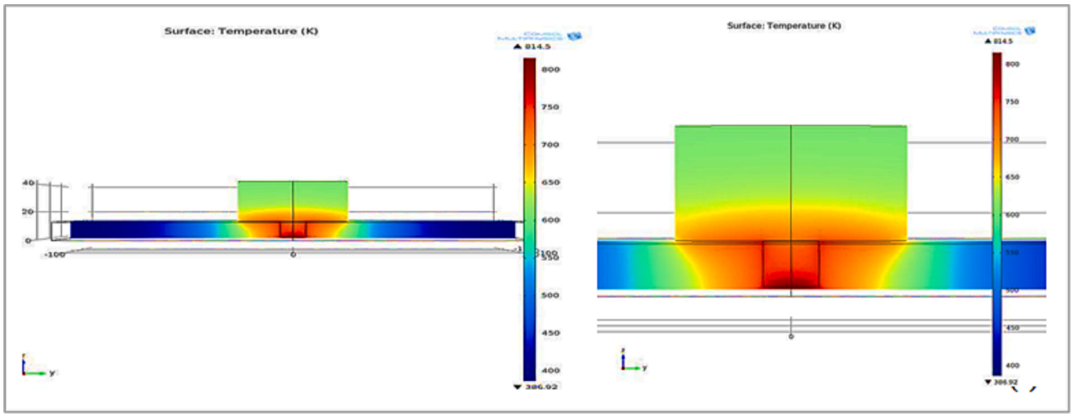

Fig. 9. Temperature distribution in the (x,z) plane and temperature distribution during Mg-Mg welding.

5. Conclusions

In this work, a numerical study was performed on COMSOL Multiphysics® software, and was made for four configuration cases: two homogeneous (AL/AL and Mg/Mg) and two heterogeneous (Al/Mg and Mg/Al). The main results obtained are as follows:

- The temperature distribution is gradual from the shoulder towards the part boundaries, and symmetrical in the middle plane (x,z) at the center of the tool. Except in the heterogeneous case where a clear

dysmetria is observed. This is due to the different thermal properties of the materials, particularly the superior thermal conductivity of aluminum.

- In the two homogeneous cases of welding, the isothermal contours are denser and weaker in values upstream compared to downstream or they widen and increase in value. On the other hand, in the heterogeneous case the differences between the isotherms are greater in the aluminum plate and we also notice the downstream thermal distribution reached is slightly shifted towards this plate, this is due to the different thermal conductivities of the two materials.
- From the numerical results, it was identified that the temperature distribution was incremented from shoulder to the borders and it was symmetrical. The calculated maximum temperatures for magnesium and aluminum were 843.7 K & 702 K, respectively.

CRediT authorship contribution statement

C.R. Mahesha: Conceptualization, Investigation, Writing – original draft. **N. Nithyanandan:** Writing – review & editing, Investigation, Formal analysis. **K.V. Pradeep Kumar:** Formal analysis, Writing – review & editing. **Ravi Kanojia:** Writing – review & editing, Validation. **Vipin Sharma:** Data curation. **R. Satheesh Raja:** Writing – review & editing. **G. Sasikala:** Supervision, Methodology.

Declaration of Competing Interest

The authors declare that they have no known competing financial interests or personal relationships that could have appeared to influence the work reported in this paper.

Data availability

Data will be made available on request.

References

[1] M.P. Jardim, R.A. Gonçalves, M.T.P. Paes, R.R. Pires, V.L.D.S. Franco, Effect of pin and hole geometry on friction repair preliminary results, Tecnol. Metal. Mater. 4 (2) (2007) 27–32.

[2] Issac Dinaharan, Radhakrishnan Ramesh, Harish Chandra Dey, Arun Kumar Bhaduri, Effect of activating flux on penetration and microstructure of tungsten inert gas-welded pure titanium grade-2 plate, The International Journal of Advanced Manufacturing Technology (2022) 121, 3399–3417.

[3] R. Ramesh, I. Dinaharan, R. Ravikumar, E.T. Akinlabi, Microstructural characterization and tensile behavior of Nd: YAG laser beam welded thin high strength low alloy steel sheets, Mater. Sci. Eng. A 780 (2020), 139178.

[4] R. Ramesh, I. Dinaharan, Ravi Kumar, E.T. Akinlabi, Microstructure and Mechanical Characterization of Friction-Stir-Welded 316L Austenitic Stainless Steels, Journal of Materials Engineering and Performance (2019) 28 (1), 498-511.

[5] S. Yaknesh, Mohammed Tharwan, Rajasekaran Saminathan, N. Rajamurugu, K. B. Prakash, undefined Ankit, Manoj Kumar Pasupathi, Atul Sarojwal, Dawit Tafesse Gebreyohannes, "Mechanical and Microstructural Investigation on AZ91B Mg Alloys with Tool Tilt Variation by Friction Stir Welding", Advances in Materials Science and Engineering, vol. 2022, Article ID 8311413, 14 pages, 2022. https://doi.org/10.1155/2022/8311413.

[6] F.W.T. Yeh, P.H.C. Pereira da Cunha, C.R.L. Lessa, T. Clarke, T. Strohaecker, Evaluation of discontinuities in A36 steel repairs with friction hydro pillar processing using different axial forces, ISIJ Int. 53 (12) (2013) 2269–2271.

[7] R. Raj Mohan, R. Venkatraman, S. Raghuraman, P. Manoj Kumar, Moti Lal Rinawa, Ram Subbiah, B. Arulmurugan, S. Rajkumar, "Processing of Aluminium-Silicon Alloy with Metal Carbide as Reinforcement through Powder-Based Additive Manufacturing: A Critical Study", Scanning, vol. 2022, Article ID 5610333, 14 pages, 2022. https://doi.org/10.1155/2022/5610333.

[8] Ramesh C, Mohammed Tharwan, P. Manoj Kumar, Dawit Tafesse Gebreyohannes, "Microstructural and Mechanical Characteristics of Pure-Cu/brass Dissimilar Joints Welded by Friction Stir Welding Using Various Process Parameters", Advances in Materials Science and Engineering, vol. 2022, Article ID 2234352, 10 pages, 2022. https://doi.org/10.1155/2022/2234352.

[9] Raj Mohan R, Venkatraman R, Raghuraman S, Manoj Kumar P, Rajneesh Sharma, undefined Ankit, Atul Sarojwal, Rajkumar S, "Influence of Planetary Ball Mill Parameters on Powder Flowability of AlSi10Mg with Niobium Carbide Using Central Composite Design (CCD)", Advances in Materials Science and Engineering, vol. 2022, Article ID 2869225, 11 pages, 2022. https://doi.org/10.1155/2022/2869225.

[10] Baosheng Z, Xiangdong J, Jiaqing C, Zong YQ. Numerical simulation onto the preliminary period of Friction Hydro Pillar Processing in Friction Stitch Welding. In: Proceedings of the International Conference on Mechanic Automation and Control Engineering – MACE; 2010 Jun 26-28; Wuhan, China. Piscataway: IEEE Conference Publications; 2010. p. 5617.

[11] R. Ramesh, I. Dinaharan, I., E.T. Akinlabi, N. Murugan, Microstructure and Mechanical Characterization of Friction-Stir-Welded Dual-Phase Brass, Journal of Materials Engineering and Performance (2018) 27 (4), 1544-1554.

[12] R. Ramesh, I. Dinaharan, Ravi Kumar, E.T. Akinlabi, Microstructure and mechanical characterization of friction stir welded high strength low alloy steels Materials Science and Engineering: A (2017) 687, 39-46.

[13] L. Cui, X. Yang, D. Wang, X. Hou, J. Cao, W. Xu, Friction taper plug welding for S355 steel in underwater wet conditions: Welding performance, microstructures and mechanical properties, Mater. Sci. Eng. A 611 (2014) 15–28.

[14] B.A. Kumar, R. Saminathan, M. Tharwan, M. Vigneshwaran, P.S. Babu, S. Ram, P. M. Kumar, Study on the mechanical properties of a hybrid polymer composite using egg shell powder based bio-filler, Mater. Today:. Proc. 69 (2022) 679–683.

[15] Kumar, P.M., Karuna, M.S., Sureshkumar, M.S., Rinawa, M.L., Sakthivel, R., Muthukumar, K. and Malavan, E.K., 2023. Evaluating the effect of magnesium oxide nanoparticles on the thermal energy storage characteristics of the inorganic PCM. Materials Today: Proceedings.

[16] S.P. Arunkumar, C. Prabha, R. Saminathan, J.A. Khamaj, M. Viswanath, C.K. P. Ivan, R. Subbiah, P.M. Kumar, Taguchi optimization of metal inert gas (MIG) welding parameters to withstand high impact load for dissimilar weld joints, Mater. Today:. Proc. 56 (2022) 1411–1417.

[17] N. Senthil Kannan, R. Parameshwaran, P.T. Saravanakumar, P.M. Kumar, M. L. Rinawa, Performance and quality improvement in a foundry industry using fuzzy MCDM and lean methods, Arab. J. Sci. Eng. 47 (12) (2022) 15379–15390.

[18] BV Ramnath, C Elanchezhian, S Rajesh, SJ Prakash, BM Kumaar, Design and development of milling fixture for friction stir welding, Materials Today: Proceedings 5 (1), 1832-1838.

[19] P. Manoj Kumar, M. Palaniappan, M. Sharma, R. Suresh, K. Parmar, R. Surakasi, D. Rana, M. Sudhakar, Modelling and analysis of an N-DPCM (nano-doped PCM) integrated solar water heater using CFD, Int. J. Interact. Des. Manuf. (IJIDeM) (2022) 1–12.

[20] Santhosh Kumar B. M, Pamula Keerthana, G.Ravi, Kumud Pant, M.Sudhakar, "Bio polymer based food packaging using composite materials," Materials Today: Proceedings, Volume 66, Part 3, 2022, Pages 834-837.

[21] T. Naresh Kumar, A.K. Saravanan, S. Shylin, H. Jose, L. Ravikumar, M. Sudhakar, Reinforcing adhesive plastic-coated grins through FRP compounds, Int. J. Eng. Adv. Technol. 9 (1) (2019) 3356–3358.

[22] D. Muruganandam, J. Jayapriya, G. Ramakrishnan, G. Puthilibai, P. Karthick, M. Sudhakar, Enhancing heat transfer rate in heat exchanger using nano particles of the natural Glay, Mater. Today:. Proc. 32 (7) (2020) 4402–4407.

[23] T.Vennila, Raviteja Surakasi, K.S.Raghuram, G.Ravi, S.Madhavarao, Chikkappa Udagani, M.Sudhakar, "Investigation on tensile behaviour of Al/Si3N4/sugarcane ash particles reinforced FSP composites," Materials Today: Proceedings, Vol. 59, no.2, pp. 1266–1270, 2022.

[24] R. Venkatesh et al., "Influence of Different Frequency Pulse on Weld Bead Phase Ratio in Gas Tungsten Arc Welding by Ferritic Stainless Steel AISI-409L", Journal of Nanomaterials, vol. 2022, Article ID 9530499, 11 pages, 2022.

[25] Naresh Kumar et al., "Development of Novel Bio-mulberry-Reinforced Polyacrylonitrile (PAN) Fibre Organic Brake Friction Composite Materials", Bioinorganic Chemistry and Applications, vol. 2022, Article ID 6426763, 11 pages, 2022.

[26] BV Ramnath, J Jeykrishnan, G Ramakrishnan, B Barath, Sea shells and natural fibres composites: a review, Materials Today: Proceedings 5 (1), 1846-1851.

[27] VR Raman, Bharath, B Vijaya Ramnath, N Manoharan, Kenaf fibre reinforced composites: a review, ARPN Journal of Engineering and Applied Sciences ,10, 5483-5485.

[28] P.S. Reddy, R. Kesavan, B. Vijaya Ramnath, Investigation of mechanical properties of aluminium 6061-silicon carbide, boron carbide metal matrix composite, Silicon 10 (2018) 495–502.

[29] Sivakumar, K, Natarajan, E, & Kulasekharan, N. "Influence of Different Rib Height on Heat Transfer Augmentation in Rectangular Convergent / Divergent Channels with Continuous Ribs on Bottom Surface." Proceedings of the ASME 2013 Gas Turbine India Conference. ASME 2013 Gas Turbine India Conference. Bangalore, Karnataka, India. December 5–6, 2013. V001T02A007. ASME.

[30] Sivakumar. K, Natarajan.E and Kulasekharan.N, 'CFD Simulation and Experimental Investigation of Convection Heat Transfer in a Rectangular Convergent Channel with Staggered Ribs', International Review of Mechanical Engineering, vol.7, no.3, 2013, pp.541-548.

[31] Sivakumar.K, Natarajan.E and Kulasekharan.N, Gas turbine blade cooling at mid chord region by using rib turbulators – a review, Journal of Mechanical Engineering (Strojnicky casopis). Vol.63 (1), 2012, pp. 1-16.

[32] K.B. Prakash, M.K. Pasupathi, S. Subramaniyan Chinnasamy, M.P. Saravanakumar, A. Alasiri, M. Chandrasekaran, Energy and exergy enhancement study on PV systems with phase change material, Sustainability 15 (4) (2023) 3627, https://doi.org/10.3390/su15043627.

[33] Sivakumar.K, Natarajan.E and Kulasekharan, N, Numerical Simulation on Rectangular Divergent Ribbed Channels, ARPN Journal of Engineering and Applied Sciences, Vol.11,no.18,2016, pp.-11023-11030.

[34] Prakash, K. B., Mohammed Almeshaal, Manoj Kumar Pasupathi, Subramaniyan Chinnasamy, S. Saravanakumar, and S. Rajesh Ruban. 2023. "Hybrid PV/T Heat

Pump System with PCM for Combined Heating, Cooling and Power Provision in Buildings" Buildings 13, no. 5: 1133. 10.3390/buildings13051133.

[35] B. Murali, N. Krishnamoorthy, P. Manoj Kumar, M. Saravanan, D. Madankumar, R. Surakasi, A. Sharma, M. Sudhakar, Design and performance optimization of a solar still using nano-coated condensing glass, Int. J. Interact. Des. Manuf. (IJIDeM) (2022) 1–6.

[36] Sivakumar.K, Natarajan.E and Kulasekharan.N, Numerical study of turbulent flow and heat transfer in square convergent channel with 90° inline rib turbulator's, International Journal of Engineering and Innovative Technology. Vol.1. (3). Pp. 218-224.